RMetS

Royal Meteorological Society

Multi-GCM by multi-RAM experiments for dynamical downscaling on summertime climate change in Hokkaido

Masaru Inatsu,[1]* Tomonori Sato,[2] Tomohito J. Yamada,[3] Ryusuke Kuno,[4] Shiori Sugimoto,[5] Murad A. Farukh,[3] Yadu N. Pokhrel[6] and Shuichi Kure[7]

[1]*Faculty of Science, Hokkaido University, Sapporo, Japan*
[2]*Faculty of Earth Environmental Sciences, Hokkaido University, Sapporo, Japan*
[3]*Faculty of Engineering, Hokkaido University, Sapporo, Japan*
[4]*ARK Information Systems, Yokohama, Japan*
[5]*Graduate School of Urban Environmental Sciences, Tokyo Metropolitan University, Japan*
[6]*Department of Civil and Environmental Engineering, Michigan State University, East Lansing, MI, USA*
[7]*International Research Institute of Disaster Science, Tohoku University, Sendai, Japan*

*Correspondence to
 M. Inatsu, Faculty of Science,
Hokkaido University, Rigaku 8th
bldg., N10W8, Sapporo
060-0810, Japan.
E-mail:
inaz@mail.sci.hokudai.ac.jp*

Abstract

The experiments with three general circulation models (GCMs) by three regional atmospheric models (RAMs) for the dynamical downscaling (DDS) have been performed to evaluate the uncertainty in the global warming response during summertime in Hokkaido, Japan. The results of a 10-year RAM integration nested into GCM under present or future climate conditions were synthesized after applying bias correction. For the target decades during which the global-mean temperature increases by 2 K in each GCM, the DDS results indicate that surface air temperature and precipitation mostly depend on the GCM imposed as the lateral boundary condition.

Keywords: dynamical downscaling; regional climate change; multi-GCM by multi-RAM experiments

1. Introduction

Researches on climate change adaptation have been widely conducted mostly as governmental or inter-governmental projects, in order to make an optimal policy to adjust society, economy, industries, and life styles to imminent dangers due to the increase in surface air temperatures (SATs), the change of precipitation, snow melting, and sea level rise by global warming. A comprehensive consideration including climate change projection, risk assessment, and decision making is required in such a project. A great hindrance on it is the uncertainty on climate change projection that is inevitable mainly for two reasons: many possible choices in our future society that may control the level of greenhouse gas emissions, and many possible choices in climate model parameterizations that cause the climate sensitivity. Moreover, although the climate change is a universal issue for human being, the adaptation processes ranging from risk assessment to decision making are indeed regional and thus need finer resolution information on the climate change. However, most general circulation models (GCMs) used in climate experiments still use a rather coarse horizontal resolution of hundreds of kilometers.

The dynamical downscaling (DDS) is a modern technique to estimate the climate change in a particular domain by running a regional atmospheric model (RAM) nested in lower-resolution boundary conditions derived from a GCM (Giorgi and Bates, 1989).

Compared with the statistical downscaling, DDS can provide a dataset in which climatic variables are mutually physical consistent, are temporally varying, and are constrained by the synoptic conditions externally given. The DDS result is often sensitive to physical parameterizations implemented in RAMs such as cloud physics, precipitation, radiative transfer, and turbulent mixing (cf. Wang *et al.*, 2004). The GCM is imposed as lateral boundary condition in a RAM experiment, which is equally sensitive to GCM's physical parameterizations. Hence, the multi-model ensemble approach has been advocated in EU ENSEMBLES (van der Linden and Mitchell, 2009), NARCCAP (Wang *et al.*, 2009), and S5-3 (Ishizaki *et al.*, 2012), to evaluate the uncertainty in the DDS estimation. Particularly an effort in the combination of multiple RAMs and multiple GCMs was devoted in EU ENSEMBLES, and the project provided a matrix for assembling their DDS results.

The uncertainty in DDS results can be classified into three aspects with different scales. First, as has been introduced above, there are many possible ways to parameterize physical processes in a RAM. Second, as the RAM is driven by the lateral boundary conditions, the result is apparently influenced by external synoptic states that are more or less uncertain in the climate change projection. Finally the global-mean SAT is highly uncertain due to the socio-economic scenario in the future and the climate sensitivity in the GCM. Without a good organization in the multi-GCM by multi-RAM experiments, however, these aspects in
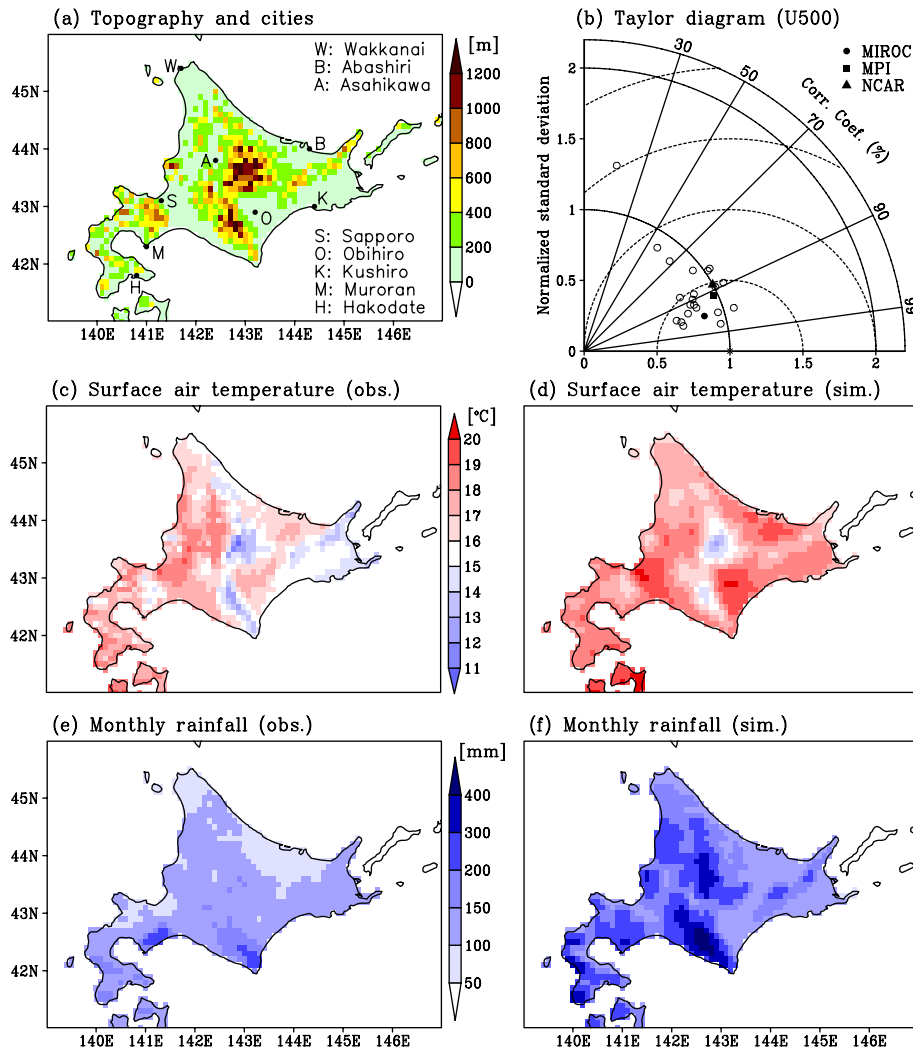
Figure 1. (a) Surface height (m) and major cities in Hokkaido labeled S (Sapporo), A (Asahikawa), H (Hakodate), K (Kushiro), O (Obihiro), M (Muroran), B (Abashiri), and W (Wakkanai). The color shading is as per the reference in the right of the panel. (b) Taylor diagram describing climatological zonal wind at 500 hPa over Northeast Asia to western North Pacific (100°–180°E by 20°–70°N) simulated by 24 models in CMIP3 compared with the observed [cross mark at (1,0)]. MIROC, MPI, and NCAR are denoted circle, square, and triangle, respectively. Standard deviation is normalized by the observed. (c) Climatological surface air temperatures (SATs) (°C) in Hokkaido in June–July–August (JJA) months based on the gridded data interpolated from 30-year Automated Meteorological Data Acquisition System (AMeDAS) observation operated by the Japan Meteorological Agency. (d) The ensemble average of SAT over all DDS experiments. (e) Climatological precipitation (mm month^{-1}) in JJA months based on APHRODITE gridded rainfall data. (f) The ensemble average of precipitation.

uncertainty would get entangled in the DDS results. For example, two DDS experiments by using different GCMs and a single RAM must bring difference in SAT increase due to climate sensitivity of GCMs and some difference in precipitation and wind vector that are probably attributed to the difference of synoptic states in the GCMs. If one added more RAMs in this case, the difference in precipitation could be caused by the difference in RAM parameterizations as well. The multi-GCM by multi-RAM experiments for DDS therefore need an arrangement to clearly separate the aspects in uncertainty, but studies along this line have not been conducted yet.

The purpose of this article is to describe the results of 3-GCM by 3-RAM experiments for DDS, certainly motivated by the EU-ENSEMBLES project. In order that the uncertainty in global-mean SATs due to a

socio-economic scenario in the future and the climate sensitivity in GCMs rules out in advance, we choose a decade during which the global-mean SATs increase by 2 K for a GCM. This article hence focuses on the uncertainty potentially caused by the RAM dynamics and physical parameterizations and the GCM boundary condition. The target domain is Hokkaido (Figure 1(a)) and season is summer, where the present climate is influenced by both dry air settled down in the north and moist air intruding from the south. The Baiu rainband is maintained in the northern fringe of the Bonin high from mid-June to mid-July and is normally dismissed in the end of July (Sampe and Xie, 2010). Because the climate change projection has much uncertainty for the position, duration, and intensity of this front due to model resolution and model parameterizations (Kosaka and Nakamura, 2011), both GCMs and RAMs might

potentially bring some uncertainty in the summer rainfall change in Hokkaido. Hence, our DDS strategy may expectedly separate agents that possibly bring uncertainty. We will apply bias correction to all DDS results before analysis for a technical reason, but this is not an essential point in this article.

2. Methods

2.1. Model and experiments

We used three GCMs referred to as MIROC [The high-resolution version of Model for Interdisciplinary Research on Climate 3.2, jointly developed by the University of Tokyo.] (Hasumi and Emori, 2004), MPI [The fifth-generation atmospheric GCM in Max-Planck-Institut für Meteorologie.] (Roeckner *et al.*, 2003), and NCAR [The Community Climate System Model version 3 in the National Center for Atmospheric Research.] (Collins *et al.*, 2006) as initial and boundary conditions. The Taylor diagram for describing climatology of mid-tropospheric jet stream around Hokkaido simulated by CMIP3 models suggested that these three GCMs reproduced the present climate almost identically (Figure 1(b)); however, MIROC did not produce climatological feature of the Okhortsk high; MPI and NCAR provided weaker rainfall over Japan; MPI moreover had a bias with northward-shifted jet stream (Figure 2). The present climate period was set as 1990–1999 in the 20th century experiment (20C3M). It is noted that, as a single decade can be representative of the present climate, 10-year average and 20-year average (1980–1999) are indiscernibly similar (not shown). The future climate period was set as 2050–2059 for MIROC, 2060–2069 for MPI, and 2080–2089 for NCAR, each of which is a decade with an increase by approximately 2 K in global-mean SATs on the Special Report on Emissions Scenarios (SRES) A1b (Meehl *et al.*, 2007). The GCM outputs including sea surface temperatures (SSTs; Figure 2(f)–(h)) were prescribed in the RAM every 6 h; the GCMs under the present climate mostly reproduced the observed SST (Figure 2(e)).

We used three RAMs referred to as NHM [Non-hydrostatic model developed by Japan Meteorological Agency and Meteorological Research Institute.] (Saito *et al.*, 2006), WRF [The Advanced Research Weather Research and Forecasting Model version 3.2.1] (Skamarock *et al.*, 2008) and RSM [The regional spectral model developed by Scripps Experimental Climate Prediction Center.] (Juang and Kanamitsu, 1994) all of which are state-of-the-art models widely used in an operational forecast or a DDS experiment. The physical parameterizations for cloud, precipitation, radiative transfer, and turbulent mixing are implemented in the RAMs with a grid-based framework in NHM and WRF or with a spectral framework in RSM (Table SI in Appendix S1, Supporting Information). The horizontal resolution was set to 10 km

and there were about 30 unequally spacing vertical levels. The domain, which is centered in Hokkaido, covered 135°–150°E and 38°–50°N. The topography was prescribed as in Figure 1(a).

For each combination of three GCMs and three RAMs, a 10-year integration is performed under the present climate condition and another 10-year integration under future climate condition (e.g. Kuno and Inatsu, 2014). Many climatic variables such as SAT and precipitation rate were hourly output, and the daily maximum and minimum temperatures were defined based on the hourly data of SAT. We interpolated the original output from RAMs into an equally spaced grid in longitude and latitude for data handling. This article only describes the results in June–July–August (JJA) months. We will represent this multi-GCM by multi-RAM result in a full 3×3 matrix.

2.2. Bias correction

Figure 1(c) shows the climatology of SAT in JJA months interpolated from the Automated Meteorological Data Acquisition System (AMeDAS) operated by the Japan Meteorological Agency. The mean SAT almost ranges from 16 to 20 °C in average, while it is lower than 15 °C in southeastern Hokkaido because of a frequent fog (Sugimoto *et al.*, 2013). The daily maximum temperature sometimes exceeds 30 °C in Sapporo, Asahikawa, and Obihiro (Table 1). The DDS basically reproduced characteristic of the present-climate temperatures with a systematic bias (Figure 1(d)). The DDS ensemble average shows a 1–2 K warm bias in SAT. We then corrected the bias in SATs for each GCM-RAM combination by offsetting the difference of its present-climate climatology between observation and DDS result. Based on the bias corrected data, we will discuss summer days defined as days with maximum temperature not lower than 25 °C, hot summer days as days with maximum temperature not lower than 30 °C, and tropical night days as days with minimum temperature not lower than 25 °C.

Figure 1(e) shows the climatology of precipitation in JJA months based on APHRODITE rainfall data (Yatagai *et al.*, 2012). The mean precipitation exceeds 200 mm month^{-1} at the mountain near Muroran and at Hidaka mountain range (west of Obihiro) because of the topological uplift for moist air. In contrast, it is about 100 mm month^{-1} along the Okhotsk Sea. The DDS reproduces the observed feature in distribution (Figure 1(f)), but the ensemble average shows a positive bias in precipitation entirely over Hokkaido. We then corrected the bias for each combination of GCM and RAM by mapping the data such that empirical cumulative density function of daily precipitation amount for the observation was matched for each calendar month with that for the DDS result under the present climate condition (Piani *et al.*, 2010). This mapping function was applied to a future-climate DDS result with the same GCM-RAM combination.
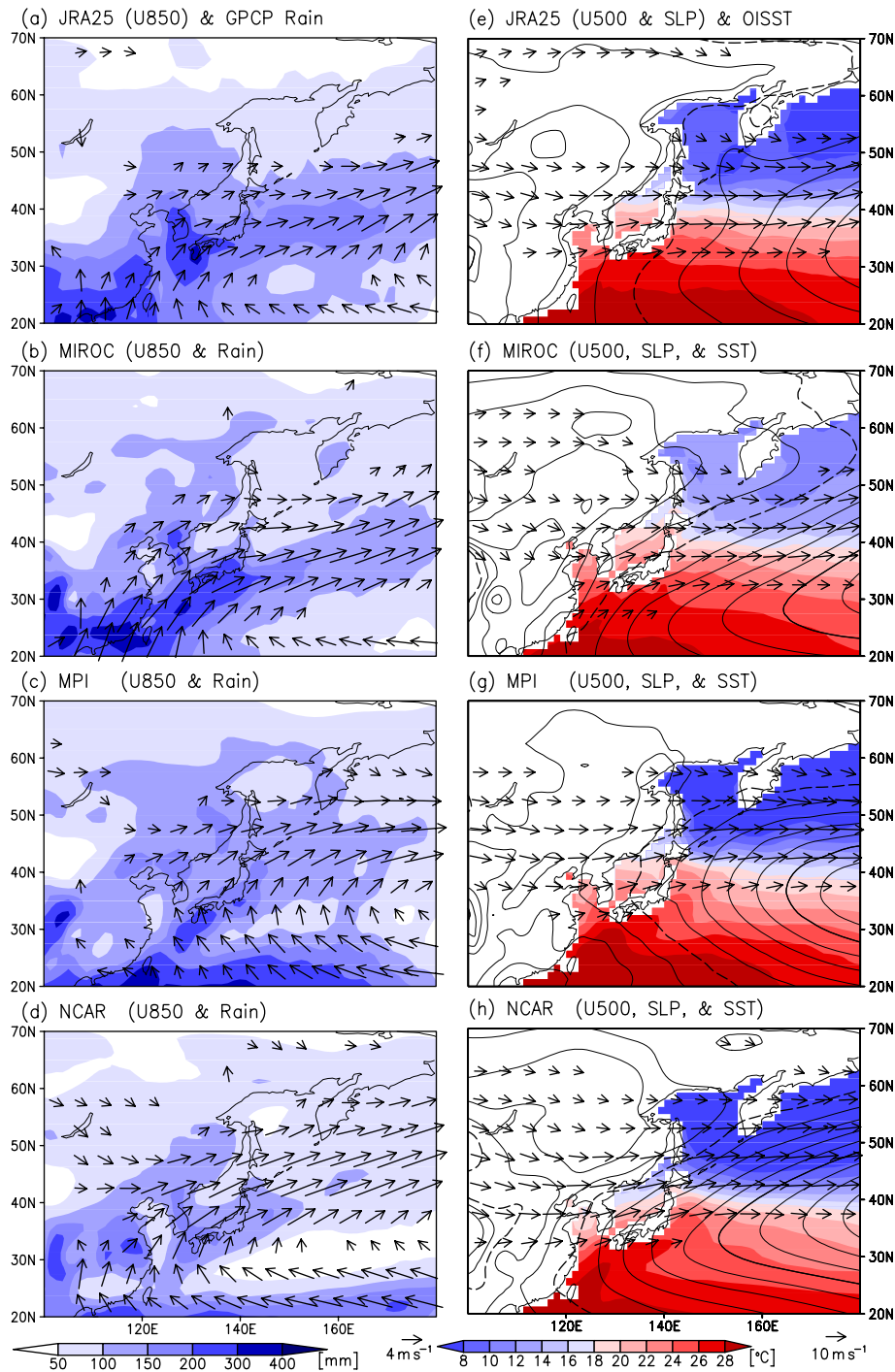
Figure 2. (a)–(d) Ten-year average of (shade) precipitation and (vector) 850-hPa horizontal wind in JJA months. The references for shading and vector are shown in the bottom. (a) The observation in 1990s based on JRA25 reanalysis and Global Precipitation Climatology Project rainfall data; result of 1990s for (b) MIROC, (c) MPI, and (d) NCAR simulations. (e)–(h) Ten-year average of (shade) sea surface temperature (SST), (contour) sea level pressure and (vector) 500-hPa horizontal wind. Contour interval is 2 hPa with a 1010 hPa contour being dotted. (e) The observation in 1990s based on JRA25 reanalysis and National Oceanic and Atmospheric Administration's Optimal Interpolated SST in 1990s; result of 1990s for (f) MIROC, (g) MPI, and (h) NCAR simulations.

3. Results

The 3×3 matrix of the DDS result of the increase in SATs in JJA months is shown in Figure 3(a). During the decade with global-mean SATs increasing by 2 K for each GCM, the temperature over Hokkaido increased by 2.5–3 K for DDS with MIROC boundary, by 2–2.5 K for DDS with MPI boundary, and 1.5–2 K

for DDS with NCAR boundary. The DDS ensemble average is thus higher than 2 K, probably because the lower heat capacity of the Eurasian continent and possibly SST distribution over the North Pacific. Moreover we found the magnitude of increase in RAM variations was relatively small for a given GCM, although the effect of topography was a bit obvious in temperature in some runs. The projection of the result onto the

Table 1. (Left column) Days per year with daily maximum temperature not lower than 25 °C, (middle) days with daily maximum temperatures not lower than 30 °C, and (right) days with daily minimum temperature not lower than 25 °C at S (Sapporo), A (Asahikawa), H (Hakodate), K (Kushiro), O (Obihiro), M (Muroran), B (Abashiri), and W (Wakkanai); cities are shown in Figure 1(a). (Left subcolumn) The days under the current climate are based on the Automated Meteorological Data Acquisition System (AMeDAS) observation. (Right subcolumn) The range of days under the future climate is based on our experiments with a bias correction.

(days year⁻¹)	$Tmax \geq 25°C$		$Tmax \geq 30°C$		$Tmin \geq 25°C$	
City	Current	Future	Current	Future	Current	Future
S	45.6	68.6−79.9	7.7	9.8−18.9	0.1	0.2−4.2
A	56.3	75.1−91.4	10.4	8.5−19.8	0.1	0.0−1.0
H	34.3	38.3−55.9	3.1	0.0−3.6	0.0	0.0−0.8
K	4.7	5.7−18.3	0.1	0.0−2.3	0.0	0.0−1.0
O	40.5	52.0−68.3	9.3	5.3−12.0	0.0	0.0−1.9
M	15.8	9.7−46.5	0.3	0.0−3.9	0.0	0.0−3.9
B	22.1	9.8−45.9	3.5	0.2−4.1	0.0	0.0−0.3
W	7.3	3.5−23.5	0.1	0.0−0.1	0.0	0.0−0.1

phase space spanned by two leading empirical orthogonal function (EOF) modes for inter-DDS variations [The EOF analysis performed for the nine DDS variations (temporal variations in an ordinary use of EOF) and we extracted main spatial patterns in DDS departure from the ensemble average.] suggested that the results with NCAR boundary were far from the others (Figure 3(b)). Among NCAR-boundary experiments, the RSM run provided a slightly different result perhaps because its dynamical core is based on a spectral method. The result above means that the GCM boundary condition mostly controls how much SAT increases in the RAM domain. Especially, a smaller SAT increase was found in the DDS with the NCAR boundary where the SST increased by smaller amounts in the subtropics (not shown).

The 3 × 3 matrix of the DDS result of the increase in precipitation in JJA months is shown in Figure 4(a). The rate of increase in precipitation was similar in RAMs for a given GCM. Only the DDS with MIROC provided many areas with a statistically significant signal
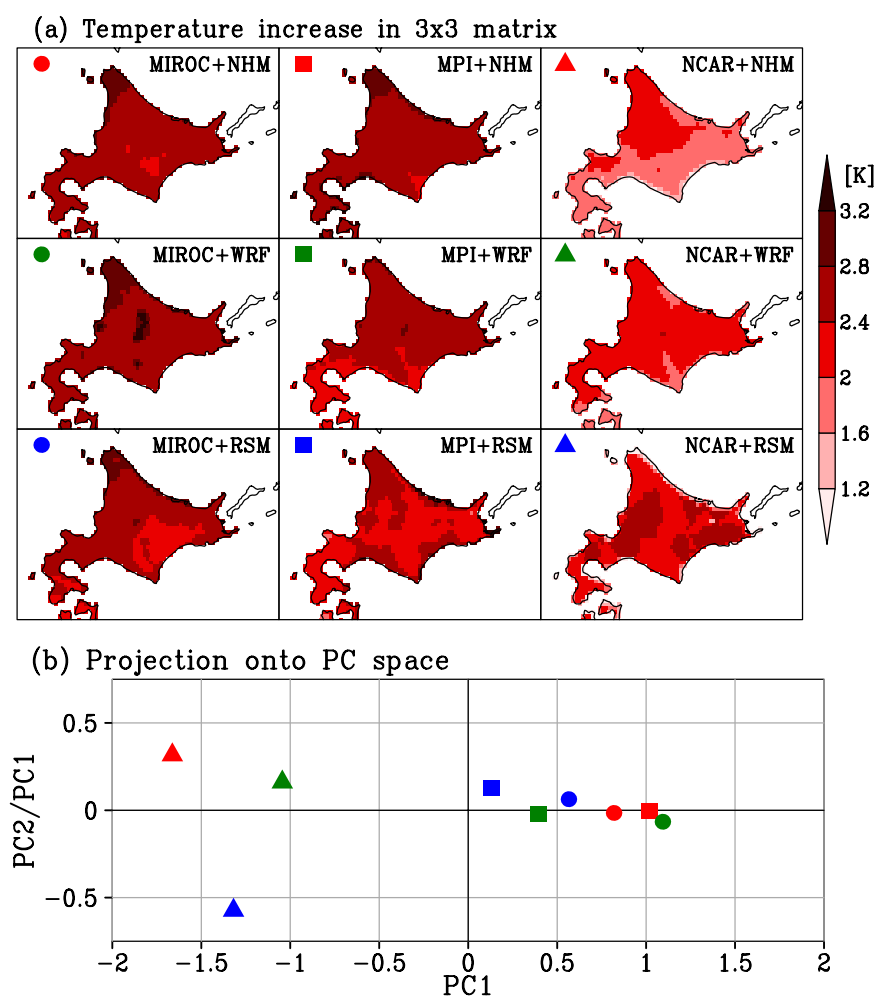

(a) Temperature increase in 3x3 matrix

(b) Projection onto PC space

Figure 3. (a) The increase in surface air temperatures (SATs) by global warming (K) with three general circulation models (GCMs) by three regional atmospheric models (RAMs) for the dynamical downscaling (DDS). The mark type and color denote the GCM-RAM combination: the mark types of circle, square, and triangle respectively mean the GCMs of MIROC, MPI, and NCAR as the lateral boundary condition; red, blue, and green, respectively, denote RAMs of NHM, WRF, and RSM. (b) The horizontal distribution for each GCM-RAM combination projected onto the phase space spanned by two leading principal components (PCs). The second PC is normalized by the ratio of the variance of PC1 to that of PC2.
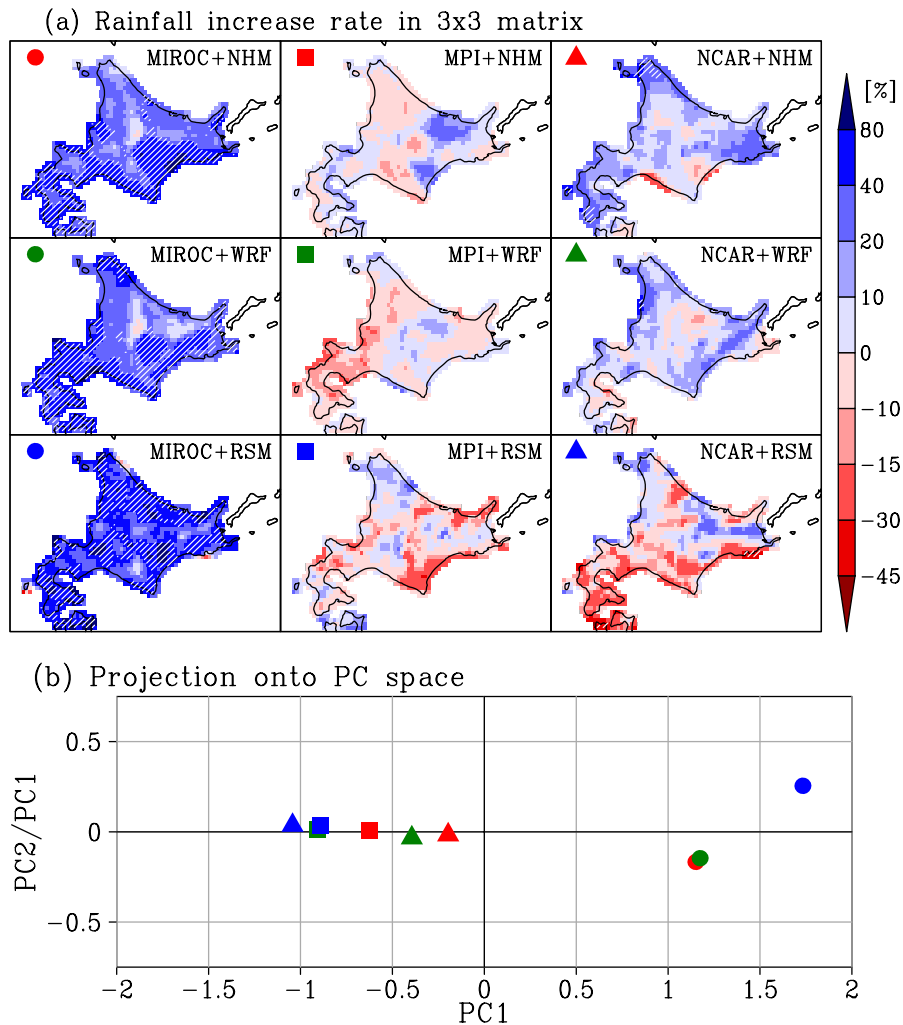
(a) Rainfall increase rate in 3x3 matrix

(b) Projection onto PC space

Figure 4. (a) The increase rate in precipitation by global warming (%) for the DDS with three-GCM by three-RAM experiments. The hatches denote areas exceeding a significant level at 10%. (b) Same as Figure 3(b), but for the horizontal distribution of the increase rate in precipitation.

while others did not (not shown). The MIROC-NHM and MIROC-WRF combinations showed a conspicuous signal with ~50% rainfall increasing in southern Hokkaido. The MIROC-RSM also showed many areas with a statistical significance but they were a bit more scattered over Hokkaido perhaps because of a different dynamical configuration in RSM. The DDS with MPI boundary provided an insignificant response in precipitation but the tendency is the decrease by ~10%. The DDS with NCAR boundary also provided an insignificant signal but the NHM and WRF runs showed a small increase and the RSM run showed a decrease in southern Hokkaido. The GCM boundary condition hence controls how much precipitation increases in the RAM domain. The projection of the results onto the phase space for inter-DDS variations supported the notion that the DDS with MIROC boundary were far from others (Figure 4(b)).

The DDS results of SAT (Figure 3) and precipitation (Figure 4) shown above suggested their strong dependency on the GCM imposed as the lateral boundary condition. In spite of GCM biases (Figure 2) and GCM parameterizations that are different from RAMs, the global warming response in GCM precipitation over Hokkaido is quite similar to DDS results (Figure 5). The MIROC provided a heavier rainfall from Northeast Asia to western North Pacific along 40°N, a bit north to the Baiu rainband in the present climate, while the MPI and NCAR did not show any significant signals there. Moreover NCAR provided a heavier rainfall just over the Baiu rainband at the present location. The precipitation response is basically related to convective instability attributed to low-level moisture flux and vertical wind shear. MIROC transported more water vapor toward Hokkaido beyond the present-climate Baiu rainband (Figure 5(a); Kimoto, 2005). The upward motion might have been induced by the tendency of upper-level jet stream confluence in the north (not shown; Horinouchi, 2014). In MPI, the anomalous wind appeared to block moist air from the south but instead encouraged the intrusion of dry air from the continent and also by northeasterly from the Okhortsk high (Figure 5(b)), associated with a bit southward shift of the upper-level jet. In NCAR, anomalous easterly was prevailed over Hokkaido and did not contribute to what the moist air straddled over the rainband in the present climate.

(a) MIROC Rainfall & VQ850 2050s/1990s
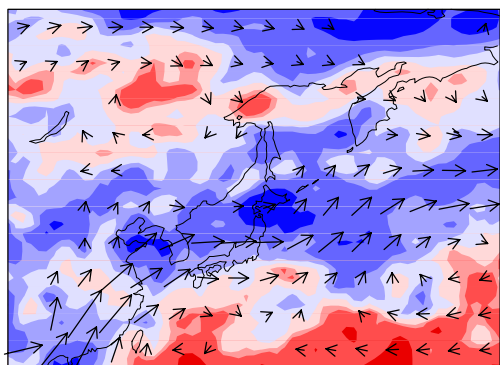
(b) MPI Rainfall & VQ850 2060s/1990s
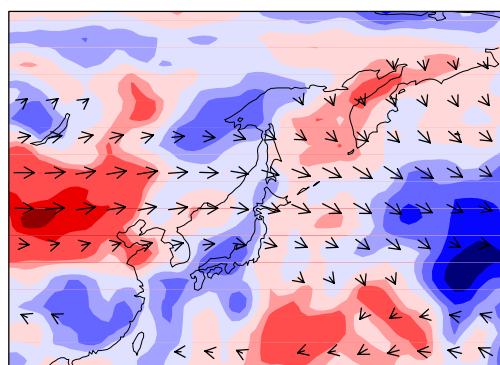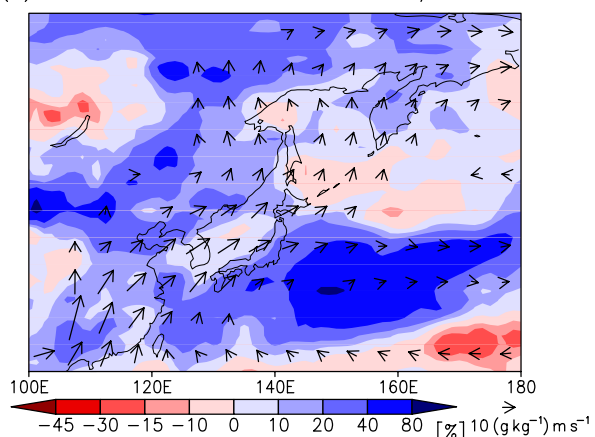
(c) NCAR Rainfall & VQ850 2080s/1990s

Figure 5. (Shade) The increase rate in precipitation and (vector) the anomalous moisture flux at 850 hPa by global warming for (a) MIROC, (b) MPI, and (c) NCAR simulations.

The moisture flux convergence was however strengthened over south of Japan. As discussed above, the DDS results (Figures 3 and 4) are basically a consequence of the synoptic-scale response to the global warming in GCM (Figure 5).

4. Conclusion and discussion

We have performed the multi-GCM by multi-RAM experiments for DDS over Hokkaido. Focusing on the summertime climate there, the DDS results of SAT and precipitation commonly suggested that the downscaling results were mostly controlled by the GCM boundary condition. All combinations of GCM and RAM increased SATs by 1.5 to 3 K over Hokkaido during the decade in which the global-mean temperature increased by 2 K. Moreover, the DDS results of precipitation were quite uncertain. The experiments with MIROC boundary condition evaluated the increase in precipitation by ∼50% over Hokkaido, while other experiments provided an insignificant signal over Hokkaido. This is probably because the global warming changed low-level moisture transport toward the north beyond the present position of the Baiu rainband only in the MIROC GCM.

The increase in summertime temperatures may affect many aspects in human activity. As the present climate in Hokkaido is cool in summer with at most ten hot summer days (Table 1), air conditioners are not mostly installed in houses, buildings, and public space. Hence, a 1.5 to 3 K temperature increase brings solely a slightly hotter climate, but children, elderly people, and health impaired would be exposed to a potential risk of the heat disorder (Ohashi *et al.*, 2014). Together with an urban effect, for example, summer days and hot summer days almost doubled and possibility of tropical night days increased in Sapporo (Table 1), which would indeed deteriorate the quality of life. Temperature increase might also impact agriculture, a major industry in Hokkaido. Cultivation of wheat, potatoes, and sugar beet, and pastoral farming tends to take damages for high temperatures over eastern Hokkaido even now. Such a risk might become higher under the future climate (e.g. Hirota *et al.*, 2011; Nishio *et al.*, 2013).

The possible increase in summer precipitation mainly affects the water resource management. Because of a less summer precipitation in Hokkaido than that in mainland, there is high flood vulnerability to the increase in precipitation even for three major rivers in Hokkaido (Yamada *et al.*, 2012). As the precipitation increases more likely in southern Hokkaido (Figure 4(a)), we can evaluate that Tokachi River has the first priority to reduce vulnerability on possible flood among three river basins.

Supporting information

The following supporting information is available:

Appendix S1. Dynamical framework and physical parameterizations in JMA, WRF, and RSM that were used in the text.

References

Collins WD, Bitz CM, Blackmon ML, Bonan GB, Bretherton CS, Carton JA, Chang P, Doney SC, Hack JJ, Henderson TB, Kiehl JT, Large WG, McKenna DS, Santer BD, Smith RD. 2006. The community climate system model version 3 (CCSM3). *Journal of Climate* **19**: 2122–2143.

Giorgi F, Bates GT. 1989. The climatological skill of a regional model over complex terrain. *Monthly Weather Review* **117**: 2325–2347.

Hasumi H, Emori S. 2004. K-1 coupled GCM (MIROC) description. K-1 Technical Report 1, CCSR, University of Tokyo: Tokyo.

Hirota T, Usuki K, Hayashi M, Nemoto M, Iwata Y, Yanai Y, Yazaki T, Inoue S. 2011. Soil frost control: agricultural adaptation to climate variability in a cold region of Japan. *Mitigation and Adaptation Strategies for Global Change* **16**: 791–802.

Horinouchi T. 2014. Influence of upper tropospheric disturbances on the synoptic variability of precipitation and moisture transport over summertime East Asia and the northwestern Pacific. *Journal of the Meteorological Society of Japan*, doi: 10.2151/jmsj.2014-602.

Ishizaki NN, Takayabu I, Ohízumi M, Sasaki H, Dairaku K, Iizuka S, Kimura F, Kusaka H, Adachi SA, Kurihara K, Murazaki K, Tanaka K. 2012. Improved performance of simulated Japanese climate with a multi-model ensemble. *Journal of the Meteorological Society of Japan* **90**: 235–254.

Juang HM, Kanamitsu M. 1994. The NMC nested regional spectral model. *Monthly Weather Review* **122**: 3–26.

Kimoto M. 2005. Simulated change of the east Asian circulation under global warming scenario. *Geophysical Research Letters* **32**: L16701.

Kosaka Y, Nakamura H. 2011. Dominant mode of climate variability, intermodel diversity and projected future changes over the summertime western North Pacific simulated in the CMIP3 models. *Journal of Climate* **24**: 3935–3955.

Kuno R, Inatsu M. 2014. Development of sampling downscaling: a case for wintertime precipitation in Hokkaido. *Climate Dynamics* **43**: 375–387.

Meehl GA, Stocker TF, Collins WD, Friedlingstein P, Gaye AT, Gregory JM, Kitoh A, Knutti R, Murphy JM, Noda A, Raper SCB, Watterson IG, Weaver AJ, Zhao Z-C. 2007. Global climate projections. In *Climate Change 2007: The Physical Science Basis*, Solomon S et al. (eds). Cambridge University Press: Cambridge, UK and New York, NY; 747–845.

Nishio Z, Ito M, Tabiki T, Nagasawa K, Yamauchi H, Hirota T. 2013. Influence of higher growing-season temperatures on the yield components on winter wheat (*Triticum aestivum* L.). *Crop Science* **53**: 621–628.

Ohashi Y, Kikegawa Y, Ihara T, Sugiyama N. 2014. Numerical simulations of outdoor heat stress index and heat disorder risk in the 23 wards of Tokyo. *Journal of Applied Meteorology and Climatology* **53**: 583–597.

Piani C, Haerter JO, Coppola E. 2010. Statistical bias correction for daily precipitation in regional climate models over Europe. *Theoretical and Applied Climatology* **99**: 187–192.

Roeckner E, Bäuml G, Bonaventura L, Brokopf R, Esch M, Giorgetta M, Hagemann S, Kirchner I, Kornblueh L, Manzini E, Rhodin A, Schlese U, Schulzweida U, Tompkins A. 2003. The atmospheric general circulation model ECHAM5. Part I: model description. MPI for Meteorol Report 349, MPI for Meteorol, Hamburg, Germany.

Saito K, Fujita T, Yamada Y, Ishida J, Kumagai Y, Aranami K, Ohmori S, Nagasawa R, Kumagai S, Muroi C, Kato T, Eito H, Yamazaki Y. 2006. The operational JMA nonhydrostatic mesoscale model. *Monthly Weather Review* **134**: 1266–1298.

Sampe T, Xie SP. 2010. Large-scale dynamics of the Meiyu-Baiu rainband: environmental forcing by the westerly jet. *Journal of Climate* **23**: 113–134.

Skamarock WC, Klemp JB, Dudhia J, Gill DO, Barker DM, Duda MG, Huang X-Y, Wang W, Powers JG. 2008. A description of the advanced research WRF version 3. NCAR Technical Note NCAR/TN-475+STR, National Center for Atmospheric Research: Boulder, CO; 113 pp.

Sugimoto S, Sato T, Nakamura K. 2013. Effects of synoptic-scale control on long-term declining trends of summer fog frequency over the Pacific side of Hokkaido Island. *Journal of Applied Meteorology and Climatology* **52**: 2226–2242.

van der Linden P, Mitchell JFB (eds). 2009. *ENSEMBLES*: *Climate Change and its Impacts*: *Summary of Research and Results from the ENSEMBLES Project*. Met Office Hadley Centre: Exeter, UK; 160 pp

Wang YQ, Leung LR, Mcgregor JL, Lee DK, Wang WC, Ding Y, Kimura F. 2004. Regional climate modeling: progress, challenges, and prospects. *Journal of the Meteorological Society of Japan* **82**: 1599–1628.

Wang SY, Gillies RR, Takle ES, Gutowski WJ. 2009. Evaluation of precipitation in the Intermountain Region as simulated by the NARCCAP regional climate models. *Geophysical Research Letters* **36**: L11704, doi: 10.1029/2009GL037930.

Yamada TJ, Sasaki J, Matsuoka N. 2012. Climatology of line-shaped rainband over northern Japan in boreal summer between 1990 and 2010. *Atmospheric Science Letters* **13**: 133–138.

Yatagai A, Kamiguchi K, Arakawa O, Hamada A, Yasutomi N, Kitoh A. 2012. APHRODITE: constructing a long-term daily gridded precipitation dataset for Asia based on a dense network of rain gauges. *Bulletin of the American Meteorological Society* **93**: 1401–1415.